

The first alkaline-earth fluorooxoborate Ba[B₄O₆F₂] - characterisation and doping with Eu²⁺

Stephan G. Jantz, Florian Pielhofer, Leo van Wüllen, Richard
Wehrich, Martin J. Schäfer, Henning A. Höpfe

Angaben zur Veröffentlichung / Publication details:

Jantz, Stephan G., Florian Pielhofer, Leo van Wüllen, Richard Wehrich, Martin J. Schäfer, and Henning A. Höpfe. 2018. "The first alkaline-earth fluorooxoborate Ba[B₄O₆F₂] - characterisation and doping with Eu²⁺." Chemistry - A European Journal 24 (2): 443-50. <https://doi.org/10.1002/chem.201704324>.

Nutzungsbedingungen / Terms of use:

licgercopyright

Dieses Dokument wird unter folgenden Bedingungen zur Verfügung gestellt: / This document is made available under these conditions:

Deutsches Urheberrecht

Weitere Informationen finden Sie unter: / For more information see:

<https://www.uni-augsburg.de/de/organisation/bibliothek/publizieren-zitieren-archivieren/publiz/>



The First Alkaline-Earth Fluorooxoborate Ba[B₄O₆F₂]—Characterisation and Doping with Eu²⁺

Stephan G. Jantz,^[a] Florian Pielhofer,^[c] Leo van Wüllen,^[b] Richard Wehrich,^[c] Martin J. Schäfer,^[a] and Henning A. Höppe^{*[a]}

Dedicated to Professor Wolfgang Schnick on the occasion of his 60th birthday

Abstract: The very first alkaline-earth fluorooxoborate Ba[B₄O₆F₂] was synthesised by solid state methods starting from Ba(BF₄)₂, β-BaB₂O₄, and B₂O₃. The crystal structure derived from single-crystal X-ray diffraction (*P*2₁/*n*, *a* = 6.6384(2) Å, *b* = 7.6733(3) Å, *c* = 11.3385(4) Å, β = 91.281(2)°, *Z* = 4, *R*_{int} = 0.0269, *R*₁ = 0.018, *wR*₂ = 0.034) comprises layers of BO₃F tetrahedra condensed through triangular BO₃ units according to the descriptor 2Δ2□: <Δ2□ > Δ. The extraordinary thirteen-fold coordination of barium by oxygen and

fluorine leads to interesting optical properties of a sample doped with divalent europium, where a 4f → 4f emission was recorded around 359 nm together with a broad emission band of a 5d → 4f emission peaking at 366 nm. The compound is further characterised by IR-, Raman-, and solid-state NMR-spectroscopic methods. Moreover, DFT calculations as well as TGA and DSC measurements were performed.

Introduction

In the course of our systematic investigations of silicate-analogous materials^[1–4] we also focus on inorganic fluoro-derivatives of oxo-anions like phosphates, borates, and tungstates.^[5] Silicate-analogous materials promise a very large structural variability known from silicate chemistry; sometimes they even comprise features not known therein. For instance, borates also allow for a trigonal planar coordination of the network building cation boron. The inorganic fluorooxoborates known so far comprise trivalent bismuth^[6,7] and mainly alkali metal as well as ammonium cations,^[8–20] which were investigated with regard to their behaviour as ionic conductors or their non-linear optical properties.

Our main focus lies on luminescent compounds, that is, phosphors, and we are therefore interested in respective compounds of divalent and trivalent cations. In this context we discovered the first representative of alkaline-earth fluorooxoborates—Ba[B₄O₆F₂]—as the existence of Ba[BOF₃] is in

doubt.^[20–22] Thus, Ba[B₄O₆F₂] is the first verified representative of this compound class, with a divalent cation suited for doping with divalent rare-earth ions. The possibility of doping rare-earth ions as activators on the barium site, as well as the sufficient thermal stability, make it a promising candidate as host structure for phosphors with interesting optical properties, since the local surrounding strongly influences the optical properties of doped divalent europium ions. In contrast to the alkali fluorooxoborates, Ba[B₄O₆F₂] shows a remarkable stability against air and moisture. Moreover, very recently, a compound of this composition has been predicted theoretically.^[23]

Results and Discussion

Crystal structure

Barium fluorooxoborate, Ba[B₄O₆F₂], crystallises in a new structure type in the monoclinic space group *P*2₁/*n* (no. 14) with four formula units per unit cell. All atoms occupy the general Wyckoff site 4e.

The anionic partial structure comprises condensed BO₃ triangles and BO₃F tetrahedra, which form corrugated layers perpendicular to [010] (Figures 1 and 2). The fundamental building unit (FBU) is a six-membered B₃O₃ ring built up by one trigonal planar BO₃ unit and two BO₃F tetrahedra, with one of them being connected to a further BO₃ triangle (Figure 3) and can be described by the descriptor 2Δ2□: <Δ2□ > Δ.^[24] Three of these FBUs form an 18-membered B₉O₉ ring with a barium atom in the center (slightly out of plane).

Concerning the FBU, the cross-linkage, and the layered structure, the crystal structure of Ba[B₄O₆F₂] is very similar to

[a] S. G. Jantz, M. J. Schäfer, Prof. Dr. H. A. Höppe
Lehrstuhl für Festkörperchemie, Universität Augsburg
Universitätsstraße 1, 86159 Augsburg (Germany)
E-mail: henning@ak-hoeppe.de

[b] Prof. Dr. L. van Wüllen
Lehrstuhl für Chemische Physik und Materialwissenschaften
Universität Augsburg, Universitätsstraße 1, 86159 Augsburg (Germany)

[c] Dr. F. Pielhofer, Prof. Dr. R. Wehrich
Lehrstuhl Chemie der Materialien und der Ressourcen
Universität Augsburg, Universitätsstraße 1, 86159 Augsburg (Germany)
Supporting information and the ORCID identification number(s) for the author(s) of this article can be found under:
<https://doi.org/10.1002/chem.201704324>

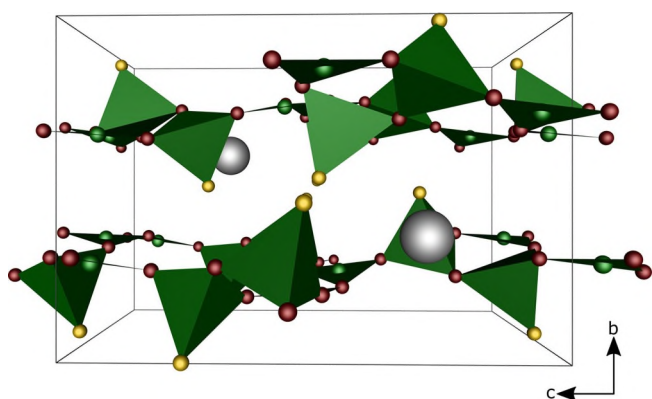


Figure 1. The layered structure of $\text{Ba}[\text{B}_4\text{O}_6\text{F}_2]$ viewed along $[1\ 0\ 0]$; barium grey, boron green, oxygen red, fluorine yellow.

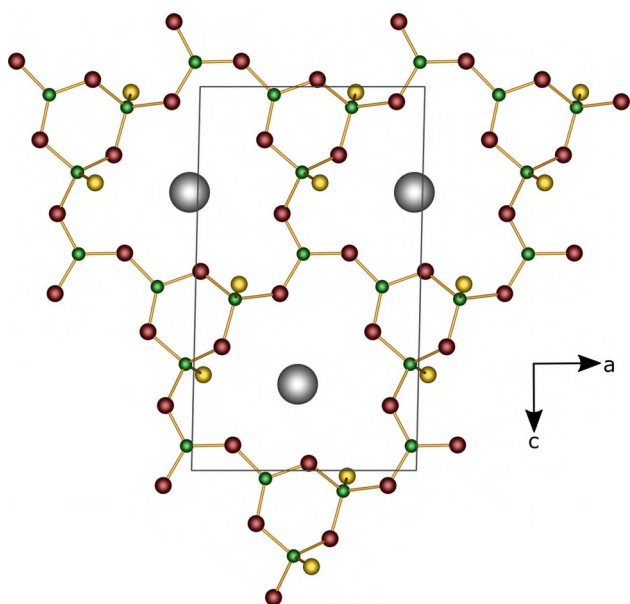


Figure 2. Single layer of $\text{Ba}[\text{B}_4\text{OF}]$ viewed along $[0\ 1\ 0]$; barium grey, boron green, oxygen red, fluorine yellow.

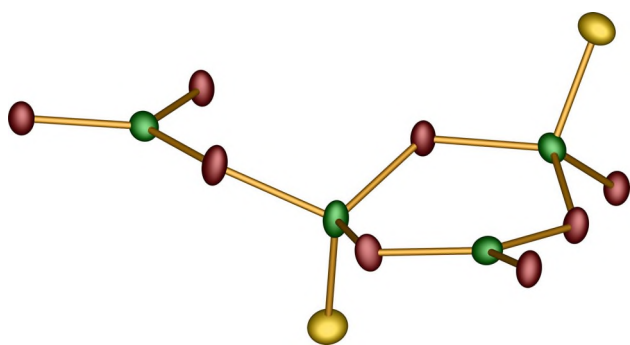


Figure 3. FBU of $\text{Ba}[\text{B}_4\text{O}_6\text{F}_2]$; boron green, oxygen red, fluorine yellow; all atoms are drawn with their displacement ellipsoids at a 75% probability level.

the rare-earth dihydroxo chloro tetraborates $\text{RE}(\text{B}_4\text{O}_6(\text{OH})_2)\text{Cl}$ ($\text{RE} = \text{Pr}, \text{Nd}$,^[25] $\text{La}, \text{Ce}, \text{Pu}$,^[26–28] all space group Cc , no. 9), which

were used as starting model to predict the structure and existence of $\text{Ba}[\text{B}_4\text{O}_6\text{F}_2]$ by Liang et al.^[23] While the fluorine atoms of the BO_3F tetrahedra in $\text{Ba}[\text{B}_4\text{O}_6\text{F}_2]$ point to both sides of the layer, in $\text{RE}(\text{B}_4\text{O}_6(\text{OH})_2)\text{Cl}$ the hydroxyl groups of the corresponding $\text{BO}_3(\text{OH})$ tetrahedra point to the same side.

The observed B–O and B–F distances (Table 1) match very well with the sum of the effective ionic radii of 1.37 Å for B–O in BO_3 , 1.49 Å for B–O, and 1.42 Å for B–F in BO_3F .^[29] The

Table 1. Relevant ranges of interatomic distances [Å] and angles [°] in $\text{Ba}[\text{B}_4\text{O}_6\text{F}_2]$ (esds in parentheses).

Ba–O _{in}	2.6676(15)–2.9710(14)
Ba–O _{out}	3.3514(15)–3.5199(14)
Ba–F	2.8915(12)–3.1828(12)
B–O _{trig}	1.358(3)–1.386(2)
B–O _{tetr}	1.447(3)–1.469(3)
B–F	1.440(2)–1.443(3)
O–B–O _{trig}	114.37(18)–123.98(17)
O–B–O _{tetr}	106.14(16)–112.53(17)
O–B–F	106.34(15)–109.43(16)

angles O–B–O and O–B–F are also close to 120° in the BO_3 triangles and 109.45° in the BO_3F tetrahedra (Table 1). With 0.25% (B1) and 0.35% (B2) the BO_3F moieties show a very small deviation from tetrahedral symmetry. These values were calculated applying the method suggested by Balić-Zunić and Makovicky, based on all ligands enclosing spheres on experimental data.^[30,31] A short description of the method has been given earlier.^[4]

The divalent barium cation is coordinated thirteen-fold by nine oxygen and four fluorine atoms, forming a distorted, singly capped icosahedron (Figure 4). The inner coordination sphere (see section Electrostatic calculations and Table S1 in the Supporting Information) consists of seven oxygen atoms with Ba–O distances in the range 2.67–2.97 Å and four fluorine atoms in distances of 2.89–3.18 Å. The outer coordination sphere includes two further oxygen atoms with distances of 3.35–3.52 Å. These coordination distances (Table 1) match with the sum of the effective ionic radii (3.03 Å for Ba–O, 2.94 Å for

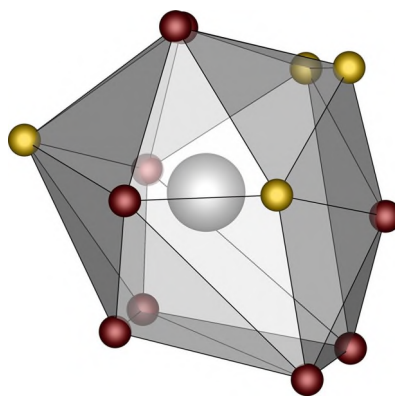


Figure 4. Coordination environment of the Ba^{2+} -ions in $\text{Ba}[\text{B}_4\text{O}_6\text{F}_2]$; barium grey, oxygen red, fluorine yellow.

Ba–F) considering that these values are tabulated only for smaller coordination spheres than the actual thirteen-fold.^[29]

Solid-State NMR spectroscopy

Although the assignment and position of the fluorine atoms is suggested from an electronic point of view, we verified the presence of covalent B–F bonds by solid-state NMR spectroscopy. Previous studies provided helpful ¹¹B data.^[32,33] The ¹¹B- and ¹⁹F-MAS NMR spectra of Ba[B₄O₆F₂] are shown in Figure 5.

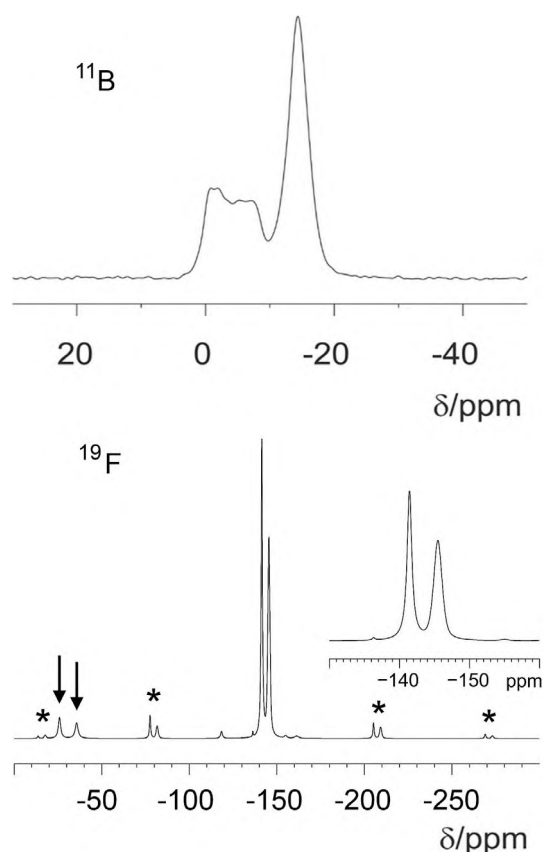


Figure 5. ¹¹B- (top) and ¹⁹F-MAS NMR spectra (bottom) of Ba[B₄O₆F₂] (* represent rotational side bands, the arrows indicate a side phase).

In the ¹¹B-MAS NMR spectrum, the broad signal in the range of –15 to –5 ppm can be assigned to boron in trigonal coordination to oxygen, whereas the signal at 0.25 ppm can be assigned to boron in tetrahedral coordination.^[34,35] In the ¹⁹F-MAS NMR spectrum we find two dominant signals at –141 and –145 ppm which we assign to the two fluorine positions in the title compound; these two signals represent approx. 86% of the total signal intensity. Signals decorated with an arrow indicate the presence of the only significant impurity phase (approx. 10% of the total intensity), those marked by asterisks denote spinning sidebands. The rotational-echo double-resonance (REDOR) experiments were performed to establish the B–F bond for the tetrahedral BO₃F units. As obvious from Figure 6a (for details please refer to the Figure caption), the tetrahedrally coordinated boron nuclei experience a considerably stronger dipolar coupling to ¹⁹F nuclei as compared to the

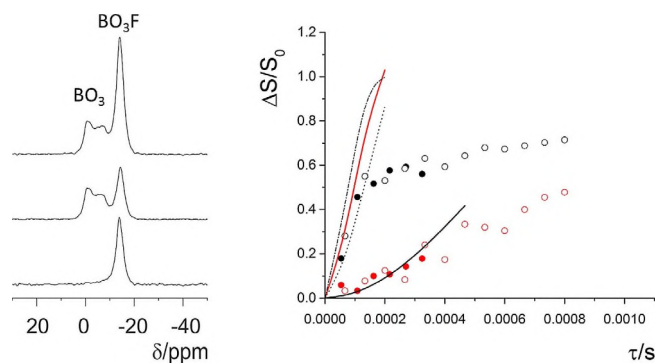


Figure 6. left: ¹¹B{¹⁹F}-REDOR-spectra for Ba[B₄O₆F₂]: top: ¹¹B spin echo; middle ¹¹B{¹⁹F}-REDOR-spectrum and bottom: difference spectrum; spectra were taken for four rotor cycles; $\nu_{\text{MAS}} = 30\,000$ Hz. The strong REDOR effect of the signal at 0.25 ppm is obvious. Right: ¹¹B{¹⁹F}-REDOR evolution curve for the ¹¹B signals for the tetrahedrally coordinated ¹¹B nuclei (black circles) and the trigonally coordinated ¹¹B nuclei (red circles); filled symbols: $\nu_{\text{MAS}} = 37\,000$ Hz; open symbols: $\nu_{\text{MAS}} = 30\,000$ Hz; lines represent results of a simulation^[36] assuming a ¹¹B-¹⁹F dipolar coupling of 1500 Hz (translating to 2.75 Å; solid black line); 6000 Hz (1.82 Å; dashed line); 8000 Hz (1.65 Å; solid red line) and 10000 Hz (1.54 Å; dashed-dotted line).

trigonally coordinated ¹¹B nuclei. Since it is not clear as to how much any impurity phases contribute to the tetrahedral and trigonal ¹¹B environments, we keep the analysis on a semi-quantitative basis. As B–F distance for the tetrahedrally coordinated ¹¹B atoms the analysis produces $r(\text{BF}) = 1.7$ Å. This, due to the mentioned uncertainty of the presence of BO₄-containing side phases, marks an upper margin for the distance, hence evidencing the presence of a direct B–F bond. The simulation for the dipolar evolution curve for the BO₃ units, on the other hand, produces a distance of 2.8 Å, in reasonable agreement with the crystal structure data. Thus, the NMR analysis clearly supports the postulated crystal structure with fluorine being present in BO₃F units.

Electrostatic calculations

We also checked our structure model of Ba[B₄O₆F₂] for electrostatic reasonability using calculations based on the MAPLE concept (MAPLE = Madelung Part of Lattice Energy).^[37–39] A structure model is considered as electrostatically consistent if the sum of MAPLE values of chemically similar compounds deviates from the MAPLE value of the compound of interest by less than 1%. According to our calculations the structure model thus shows electrostatic consistency (Table 2). Furthermore, the assignment of elements (here: oxygen and fluorine) to atomic positions can be evaluated by consideration of their partial MAPLE factors (PMF). Bridging oxygen atoms in known fluorooxoborates exhibit PMF values of 690–800 kJ mol^{–1}, while terminal fluorine atoms feature significantly lower values of 160–190 kJ mol^{–1} due to their lower charge and longer bonding distance. The PMFs in Ba[B₄O₆F₂] fit very well to these value ranges (oxygen: 714–747 kJ mol^{–1}; fluorine: 159–175 kJ mol^{–1}). Also the contribution of the outer oxygen atoms to the coordination environment of Ba was confirmed by MAPLE (Table S1).

Table 2. Result of the MAPLE calculations for Ba[B ₄ O ₆ F ₂] compared with the MAPLE calculations on BaF ₂ (ICSD no. 64717) ^[40] and B ₂ O ₃ (ICSD no. 36066). ^[41]	
MAPLE (Ba[B ₄ O ₆ F ₂])	45887
MAPLE (BaF ₂)	2608
MAPLE (B ₂ O ₃)	21586
MAPLE (BaF ₂ + 2B ₂ O ₃)	45780
Δ	0.23%

DFT calculations

Full structural optimisations, including all lattice parameters (a , b , c , β) and atomic positions, were performed with LDA and PBE functionals with additional dispersion correction to the latter. As expected, the cell volume is underestimated by 4% at the LDA level and overestimated by 8% with the PBE xc-functional. Dispersion corrected PBE calculations (PBE + D2) yield a much better result, as the cell volume is only slightly overestimated by 0.5% (Table S3). On the basis of the PBE + D2 results, the electronic density of states (DOS, Figure 7) and band structure (Figure S1) were calculated.

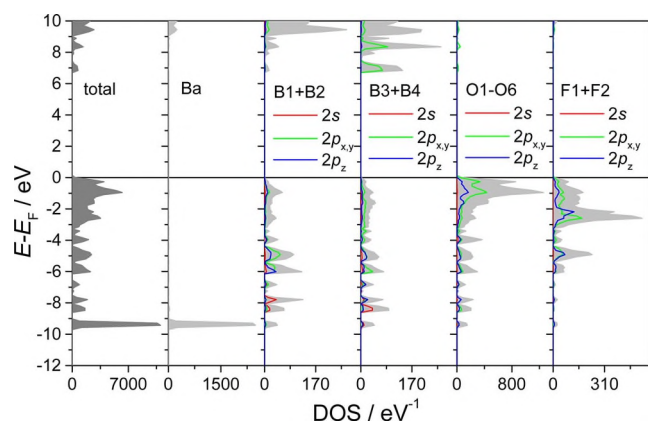


Figure 7. Total and projected DOS of Ba[B₄O₆F₂]; B1 and B2 are coordinated tetrahedrally (BO₃F), B3, and B4 trigonal planar (BO₃); O1–O6 is the sum over all oxygen sites.

Ba[B₄O₆F₂] is an insulator with a large indirect band gap of 6.8 eV. A fully ionic description of Ba (Ba²⁺) can easily be concluded from the DOS; unoccupied 6s-states are found at +9 eV above the Fermi level and only occupied 5p-states at approx. -9 eV are visible below E_F . From the top of the valence band to -3 eV O- and F-2p-states are the dominating contributions. The projected DOS (Figure 7) also allows for distinguishing between the tetrahedral BO₃F and trigonal planar BO₃ building units: A higher DOS from -5 to -6 eV is present for the tetrahedrally coordinated B1 and B2 that indicates bonding to F atoms and higher 2p_{x,y} orbital contributions from 0 to -4 eV indicate sp²-hybridisation in B3 and B4. Further, the conduction band is mainly composed of anti-bonding B3- and B4-2p_x and 2p_y-states resulting from the planar BO₃ units.

Infrared and Raman spectroscopy

The IR spectrum of Ba[B₄O₆F₂] (Figure 8) proves the absence of hydroxyl groups. $\nu_{as}(\text{BO}_3)$ vibrations emerge in the region 1390–1290 cm⁻¹, the $\nu_s(\text{BO}_3)$ band at 911 cm⁻¹. The vibrations

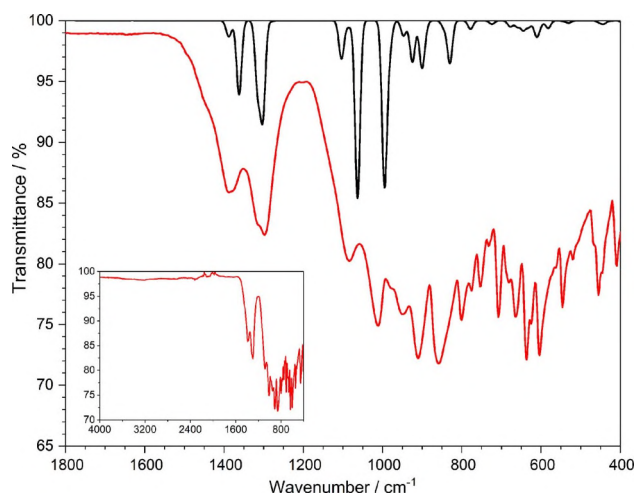


Figure 8. Observed (red) and calculated (black) IR spectra of Ba[B₄O₆F₂]; the inset shows the full recording range.

in BO₃F are induced at 1100–1000 ($\nu_{as}(\text{B-O})$), 980–940 ($\nu(\text{B-F})$), and 860–800 cm⁻¹ ($\delta(\text{BO}_3\text{F})$, $\nu_s(\text{B-O})$, $\nu(\text{B-F})$). All observed and calculated bands in the region 1400–800 cm⁻¹ and their respective assignment to the corresponding vibrations (derived from DFT calculations) are summarised in Table 3. The powder Raman spectrum of Ba[B₄O₆F₂] is depicted in Figure 9. In consequence of the multitude of bands and the shift between observed and calculated band positions, we omit an assignment here.

Table 3. Observed IR band positions [cm⁻¹] of Ba[B₄O₆F₂] and the respective values and assignments derived from DFT calculations.

Infrared	DFT	Assignment
1387 (m)	1362	$\nu_{as}(\text{BO}_3)$
1316 (sh)	1315	$\nu_{as}(\text{BO}_3)$
1298 (m)	1302	$\nu_{as}(\text{BO}_3)$
1084 (m)	1063	$\nu_{as}(\text{B-O})$ in BO ₃ F
1012 (s)	995	$\nu_{as}(\text{B-O})$ in BO ₃ F
979 (w)	947	$\nu(\text{B-F})$ in BO ₃ F
949 (w)	924	$\nu(\text{B-F})$ in BO ₃ F
911 (s)	901	$\nu_s(\text{BO}_3)$
859 (s)	830	$\delta(\text{BO}_3\text{F})$; $\nu_s(\text{B-O})$, $\nu(\text{B-F})$ in BO ₃ F
802 (m)	778	$\nu_s(\text{B-O})$, $\nu(\text{B-F})$ in BO ₃ F

Thermal analysis and stability

The thermal stability of Ba[B₄O₆F₂] was examined by thermogravimetric analysis (Figure 10) and differential scanning calorimetry (Figure 11). Ba[B₄O₆F₂] is stable up to 580 °C before decomposition starts. Both, TGA and DSC, show a signal in the

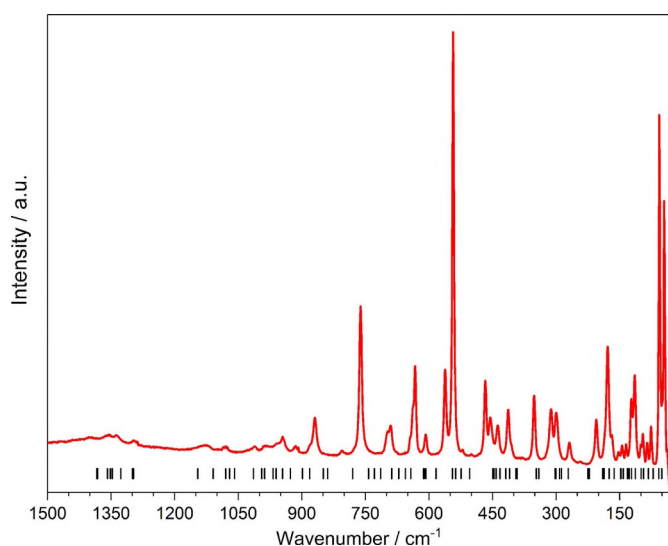


Figure 9. Observed powder Raman spectrum (red) of $\text{Ba}[\text{B}_4\text{O}_6\text{F}_2]$; calculated band positions are displayed as vertical lines.

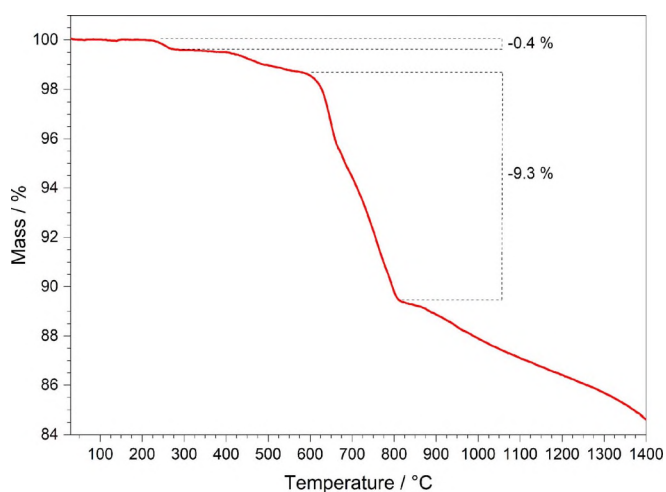


Figure 10. TG analysis ($50 \text{ mL min}^{-1} \text{ N}_2$, 10 °C min^{-1}) of $\text{Ba}[\text{B}_4\text{O}_6\text{F}_2]$ in the temperature region $30\text{--}1400 \text{ °C}$.

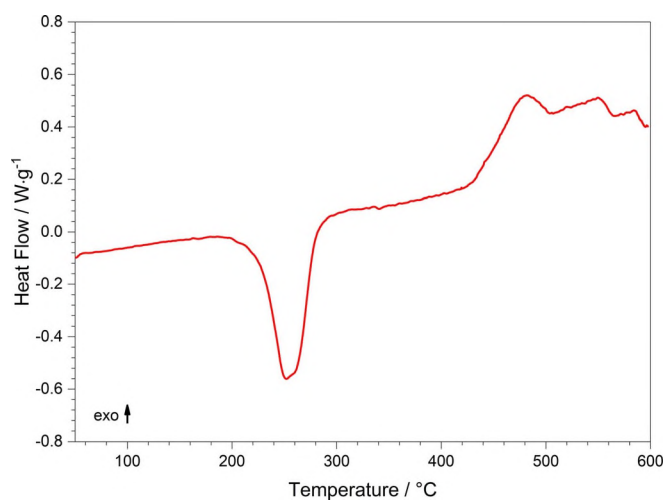


Figure 11. DSC signal ($50 \text{ mL min}^{-1} \text{ N}_2$, 10 °C min^{-1}) of $\text{Ba}[\text{B}_4\text{O}_6\text{F}_2]$ in the temperature region $50\text{--}600 \text{ °C}$.

range $210\text{--}290 \text{ °C}$ which can be related to the decomposition of H_3BO_3 and release of H_2O thereof. The investigated sample was stored in air for ten months, within which traces of unreacted starting material B_2O_3 were hydrolysed (cf. XRD data). Between $580\text{--}810 \text{ °C}$ $\text{Ba}[\text{B}_4\text{O}_6\text{F}_2]$ decomposes to the known borate fluoride $\text{Ba}_4[\text{B}_{11}\text{O}_{20}]\text{F}$.^[42] The mass loss continues up to 1400 °C where still no plateau of constant mass is reached, probably due to evaporation of B_2O_3 from the molten sample. The DSC measurement does not show any indication for a phase transition. The title compound is insensitive to air and moisture at room temperature, but decomposes to BaF_2 and H_3BO_3 if suspended in water; heating in air above 810 °C yields $\text{Ba}_4[\text{B}_{11}\text{O}_{20}]\text{F}$.^[42]

Optical properties

Doping with 5 mol.% EuF_3 during the synthesis results in Eu^{2+} luminescence in the UV region (Figure 12). If excited around 290 nm two bands are observed, the typical broad-banded $5d\text{-}4f$ and furthermore a narrow-banded $4f\text{-}4f$ emission, which can be deconvoluted as shown in Figure 12. The expected usual $f\text{-}d$ transition is centred at 366 nm , the rarely observed $f\text{-}f$ transition of Eu^{2+} (${}^6\text{P}_{7/2} \rightarrow {}^8\text{S}_{7/2}$) is centred at 359 nm , which is known for some fluorides and very few oxides.^[43,44] The ligand-field around the barium position, on which the doped europium ions should be situated, is apparently very weak, and so is the nephelauxetic effect. In contrast to other examples, this is to the best of our knowledge the first example, where for an Eu^{2+} doped compound, which is not a fluoride, both, broad-band $5d \rightarrow 4f$ and narrow-band $4f \rightarrow 4f$ emission (${}^6\text{P} \rightarrow {}^8\text{S}$), can be monitored at room temperature. This may be due to the polymeric anion which is less active for vibrational relaxation compared to other examples. The only case, in which such a behaviour was observed before, are the perovskite type compounds $\text{AMgF}_3:\text{Eu}^{2+}$ ($\text{A} = \text{Na}, \text{K}, \text{Rb}, \text{Cs}$),^[45] where the ${}^6\text{P} \rightarrow {}^8\text{S}$

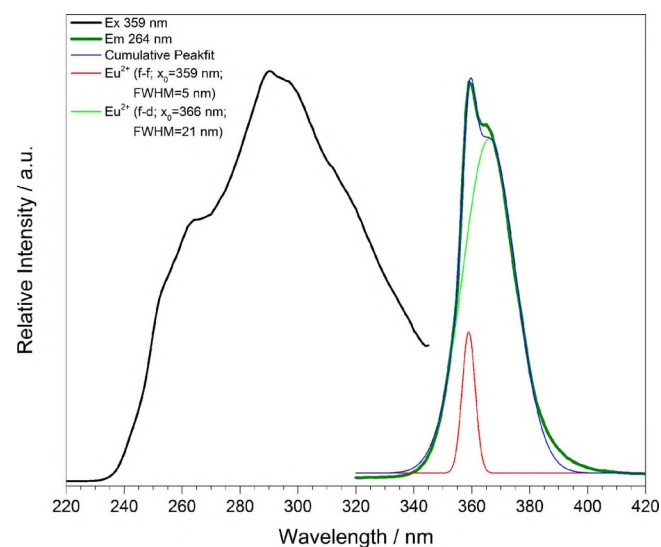


Figure 12. Absorption (black) and emission (olive) spectra of $\text{Ba}[\text{B}_4\text{O}_6\text{F}_2]:\text{Eu}^{2+}$. The emission spectrum can be deconvoluted into an $\text{Eu}^{2+}f\text{-}d$ (green) and an $\text{Eu}^{2+}f\text{-}f$ (red) emission.

emission was observed between 360 and 365 nm. Thus indeed fluoroxyborates can be classified as weakly coordinating host structures comparable with fluorides.

Conclusions

In this contribution we report on the successful synthesis of an almost phase-pure sample of the very first alkaline-earth fluoroxyborate $\text{Ba}[\text{B}_4\text{O}_6\text{F}_2]$; according to a Rietveld refinement (Figure 13, Table S2) the weight fraction of the title compound

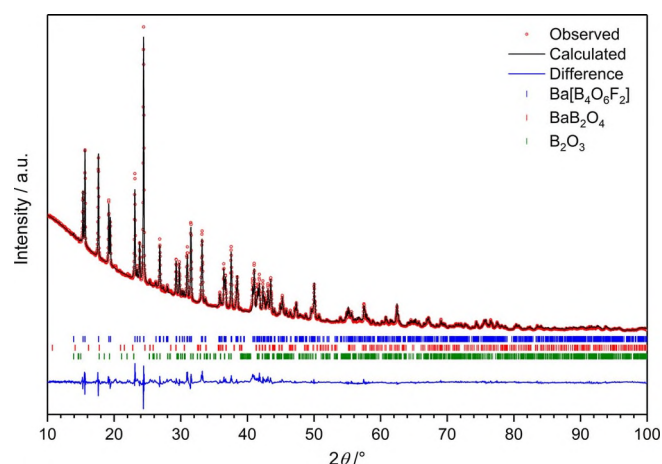


Figure 13. Observed (red circles) and calculated (black line) X-ray diffraction pattern as well as the difference profile (blue line) of the Rietveld refinement of $\text{Ba}[\text{B}_4\text{O}_6\text{F}_2]$; the rows of vertical lines indicate possible Bragg reflection positions of $\text{Ba}[\text{B}_4\text{O}_6\text{F}_2]$ (blue), BaB_2O_4 (red) and H_3BO_3 (green).

amounts to 95.5(8)%. We elucidated its crystal structure comprising a new structure type and doped it with divalent europium ions. On this pathway several questions had to be addressed; especially the unequivocal localisation of the fluorine atoms is challenging as O and F are hard to distinguish by X-ray diffraction. Based on theoretical calculations, electrostatic calculations, and solid-state NMR experiments, we could assign fluorine to the terminal positions of the BO_3F tetrahedra in the polyanion and actually prove the presence of B–F bonds. Thus both oxygen and fluorine atoms coordinate to barium, or doped europium atoms, respectively. The latter face an extremely weak coordination field strength, electrostatically and with regard to covalency. As consequence, we were able to observe not only a broad-band emission at rather short wavelengths but also even narrow-band 4f–4f (${}^6\text{P} \rightarrow {}^8\text{S}$) emission of Eu^{2+} . Fluoroxyborates can thus be classified as weakly coordinating host structures comparable with fluorides. Finally, we could also assign the infrared modes to vibrations of the lattice further confirming the crystal structure. Interestingly, $\text{Ba}[\text{B}_4\text{O}_6\text{F}_2]$ is very stable in air and up to 580 °C before it starts to decompose to known products. $\text{Ba}[\text{B}_4\text{O}_6\text{F}_2]$ is also stable against humidity as proven by powder diffractometry. Since our experimentally determined crystal structure of the title compound differs significantly from the predicted one^[23] (non-centrosymmetric space group *Cc*) it takes no wonder that cen-

trosymmetric $\text{Ba}[\text{B}_4\text{O}_6\text{F}_2]$ does not show non-linear optical properties and is therefore also not a promising NLO material.

Experimental Section

Synthesis

$\text{Ba}[\text{B}_4\text{O}_6\text{F}_2]$ was synthesised from $\text{Ba}(\text{BF}_4)_2$, $\beta\text{-BaB}_2\text{O}_4$, and B_2O_3 in the ratio 3:3:8. Inside an argon glovebox the starting materials were weighed, ground using an agate mortar, and pressed to a pellet using a self-made hand screw-press. This pellet was placed in an open silver crucible and transferred into a silica ampoule, which was evacuated at 150 °C overnight and finally sealed at a pressure of 3.4×10^{-2} mbar. The sample was fired to 550 °C with a heating rate of 50 °C h⁻¹, held at this temperature for 50 h, and cooled to room temperature with 10 °C h⁻¹.

The starting material $\text{Ba}(\text{BF}_4)_2$ was synthesised from BaCO_3 (99+ %, Aldrich), which was suspended in H_2O and treated with a substoichiometric amount of HBF_4 (ca. 50 wt.% in H_2O , Alfa Aesar). After filtration the filtrate was evaporated to dryness under vacuum and the obtained colourless powder was further dried in vacuum at 120 °C. Phase purity and the absence of water were checked by powder X-ray diffraction and IR spectroscopy. $\beta\text{-BaB}_2\text{O}_4$ was obtained from $\text{BaCl}_2 \cdot 2\text{H}_2\text{O}$ (99%, Merck), NaOH (p.A., AppliChem), and H_3BO_3 (cryst. extra pure, Merck) based on the method of Qu et al. with an additional heat treatment at 700 °C in air.^[46] B_2O_3 (99.999%, Alfa Aesar) was used as received. Attempts to gain the product from mixtures of BaF_2 and B_2O_3 or from $\text{Ba}(\text{BF}_4)_2$ and B_2O_3 were not successful.

Crystal structure determination

A colourless, plate shaped crystal with dimensions 0.060 × 0.015 × 0.040 mm was selected under an optical microscope and cooled to 130 K at a rate of 25 K h⁻¹. Single-crystal X-ray diffraction data were collected on a Bruker D8 Venture diffractometer equipped with a SMART APEXII 4k CCD detector, using $\text{MoK}\alpha$ radiation; the data were corrected for absorption by applying a multi-scan approach. The crystal structure of $\text{Ba}[\text{B}_4\text{O}_6\text{F}_2]$ was solved by direct methods, using the SHELXTL program package^[47] and refined with anisotropic displacement parameters for all atoms; the assignment of fluorine and oxygen atoms was based on different bond-lengths and positions within the BO_3F tetrahedra and proven by careful solid state NMR measurements. Details of the X-ray data collection are summarised in Table 4. The positional and displacement parameters for all atoms are listed in the Supporting Information (Tables S4 and S5); further details of the crystal structure investigation of $\text{Ba}[\text{B}_4\text{O}_6\text{F}_2]$ may be obtained from the Fachinformationszentrum Karlsruhe, D-76344 Eggenstein-Leopoldshafen, Germany (e-mail: crysdata@fiz-karlsruhe.de) on quoting the depository number CSD-433589, the names of the authors, and citation of this publication.

Powder X-ray diffraction

The powder X-ray diffraction pattern of $\text{Ba}[\text{B}_4\text{O}_6\text{F}_2]$ is shown in Figure 13. The multi-phase Rietveld refinement yielded tiny weight-contents of BaB_2O_4 (0.6(1) %) and H_3BO_3 (3.9(5) %), remaining from the starting materials BaB_2O_4 and B_2O_3 , as well as a weight fraction of 95.5(8) % of the title compound; boric acid was formed by hydrolysis of boron oxide which proves the presence of this flux in the final product—otherwise hidden in the background. Further details of the Rietveld refinement are presented in Table S2. Moreover, our measurement demonstrates that $\text{Ba}[\text{B}_4\text{O}_6\text{F}_2]$

Table 4. Crystal data and details of structure refinements.	
	Ba[B ₄ O ₆ F ₂]
temperature [K]	130(2)
<i>M</i> [g mol ⁻¹]	314.58
crystal system	monoclinic
space group	<i>P</i> 2 ₁ / <i>n</i>
<i>a</i> [Å]	6.6384(2)
<i>b</i> [Å]	7.6733(3)
<i>c</i> [Å]	11.3385(4)
β [°]	91.281(2)
<i>V</i> [Å ³]	577.42(4)
<i>Z</i>	4
$\rho_{\text{X-ray}}$ [g cm ⁻³]	3.619
crystal dimensions [mm]	0.060 × 0.015 × 0.040
color & shape	colorless plate
μ [mm ⁻¹]	6.910
<i>F</i> (000)	568
radiation λ [Å]	Mo _{Kα} 0.71073
diffractometer	Bruker D8 Venture
abs. corr.	multi-scan
min/max transmission	0.6422/ 0.7494
index range	± 9/ ± 10/ ± 15
θ range	3.21–30.00
collected reflns/indexed data	13198/1687
parameter/restraints	118/0
observed reflns (<i>I</i> > 2 σ)/ <i>R</i> _{int}	1529/0.0269
<i>R</i> (all data)	<i>R</i> ₁ = 0.018, <i>wR</i> ₂ = 0.034
weighting scheme	$w^{-1} = \sigma^2 F_o^2 + (0.0213P)^2 + 0P$; $P = (F_o^2 + 2F_c^2)/3$
Goof	1.069
min/max residual density [e ⁻ Å ⁻³]	−0.39/ 0.98

is stable against humidity. At the time of data acquisition this sample had been stored in air for ten months. The pattern was recorded on a Seifert XRD T/T 3003 diffractometer equipped with a Meteor 1D linear detector, using Cu_{K α} radiation.

Density functional theory calculations

Quantum chemical calculations were performed in the framework of density functional theory (DFT) using a linear combination of Gaussian-type functions (LCGTF) Scheme as implemented in CRYSTAL14.^[48,49] The total energy calculations including full structural optimisations were performed with the GGA (PBE)^[50] and LDA (VWN) xc-functional.^[51] Because of the layered nature of the compound and a better reproduction of experimental lattice constants, the van der Waals correction developed by Grimme was applied to PBE calculations.^[52] The convergence criterion considering the energy was set to 1×10^{-8} a.u. with a k-mesh sampling of $4 \times 4 \times 4$. Optimised all-electron basis sets were used for B,^[53] O,^[54] and F^[55] and a pseudo potential Hay–Wadt small core basis set was applied for Ba.^[56] Vibrational frequency calculations with IR intensities were run on fully optimised structural models so that no imaginary frequency was obtained. Dispersion corrected (D2) PBE calculations yielded the best results, due to well-reproduced atomic distances. The IR spectrum was simulated with the J-ICE application^[57] and the plot was fitted to Gaussian functions. For the Raman spectrum, only the band positions were calculated.

Spectroscopy

Solid-state NMR spectroscopy: ¹⁹F and ¹¹B MAS NMR spectra were recorded on a Varian VNMRs 500 NMR spectrometer with Larmor frequencies of 470.6 MHz (¹⁹F) and 160.37 MHz (¹¹B) at a spinning

speed of 30 kHz, employing a Varian 1.6 mm MAS-NMR probe. $\pi/2$ pulse lengths of 2.1 μ s (¹⁹F) or 1.2 μ s (¹¹B) were used. The ¹⁹F spectra are referenced to CFC₃, the ¹¹B spectra to BF₃·Et₂O. Spectra were recorded using a saturation comb (15 $\pi/2$ pulses spaced by 5 ms) prior to the single pulse acquisition, with recycle delays of 120 s. The presence of B–F bonds was checked employing ¹¹B{¹⁹F}-REDOR NMR spectroscopy, which enables the determination of the heteronuclear ¹¹B–¹⁹F dipole coupling and hence the evaluation of internuclear distances. In short, the result from a rotor-synchronised spin-echo experiment for the observed (¹¹B) nuclei defines the full echo intensity *S*₀. This is then compared to a spectrum resulting from an experiment in which the heteronuclear dipolar coupling between the nuclei ¹¹B and ¹⁹F has been reintroduced through rotor-synchronised π pulses (¹⁹F-channel) in addition to the ¹¹B spin-echo pulses. The difference of the spectra from the two experiments then only contains contributions from ¹¹B nuclei experiencing a dipolar coupling to ¹⁹F nuclei. The magnitude of the REDOR effect depends on the strength of the dipolar coupling and the dipolar evolution time, the latter of which can be controlled by the number of rotor cycles and the MAS frequency. The resulting REDOR evolution curves can then be analysed to evaluate the ¹¹B–¹⁹F internuclear distance.

IR spectra were recorded on a Bruker EQUINOX 55 FT-IR-Spectrometer equipped with a Platinum ATR unit in the range 4000–400 cm⁻¹ with a resolution of 4 cm⁻¹ and 32 scans.

Raman spectra were recorded on a Thermo Scientific DXR Raman-Microscope in the range 1850–35 cm⁻¹ using a 532 nm laser operated with 10 mW power. The sample was illuminated for 600 s (10-fold magnification, 50 μ m pinhole aperture, high resolution grating (1800 lines mm⁻¹), spectral resolution 1 cm⁻¹).

Fluorescence excitation and emission spectra were recorded on a Horiba Fluoromax-4 spectrometer, scanning a range from 200 to 800 nm.

Thermal analysis

The TG curve was recorded on a Netzsch STA 409 PC Luxx in a 50 mL min⁻¹ N₂ flow using an Al₂O₃ crucible. The DSC measurement was undertaken on a TA Instruments DSC 2920 in a 50 mL min⁻¹ N₂ flow using a Netzsch standard Al pan with pierced lid.

Conflict of interest

The authors declare no conflict of interest.

- [1] H. A. Höpfe, *Solid State Sci.* **2005**, *7*, 1209.
- [2] H. A. Höpfe, *Z. Anorg. Allg. Chem.* **2005**, *631*, 1272.
- [3] H. A. Höpfe, S. J. Sedlmaier, *Inorg. Chem.* **2007**, *46*, 3467.
- [4] H. A. Höpfe, *J. Solid State Chem.* **2009**, *182*, 1786.
- [5] S. G. Jantz, L. van Wüllen, A. Fischer, E. Libowitzky, E. J. Baran, M. Weil, H. A. Höpfe, *Eur. J. Inorg. Chem.* **2016**, 1121.
- [6] L. Li, G. Li, Y. Wang, F. Liao, J. Lin, *Chem. Mater.* **2005**, *17*, 4174.
- [7] R. Cong, Y. Wang, L. Kang, Z. Zhou, Z. Lin, T. Yang, *Inorg. Chem. Front.* **2015**, *2*, 170.
- [8] G. Cakmak, Dissertation, Max-Planck-Institut für Festkörperforschung, Stuttgart, **2009**.
- [9] G. Cakmak, J. Nuss, M. Jansen, *Z. Anorg. Allg. Chem.* **2009**, *635*, 631.
- [10] T. Pilz, M. Jansen, *Z. Anorg. Allg. Chem.* **2011**, *637*, 2148.
- [11] T. Pilz, H. Nuss, M. Jansen, *J. Solid State Chem.* **2012**, *186*, 104.

- [12] T. Pilz, M. Jansen, *Z. Anorg. Allg. Chem.* **2012**, 638, 1624.
- [13] G. Cakmak, T. Pilz, M. Jansen, *Z. Anorg. Allg. Chem.* **2012**, 638, 1411.
- [14] B. Andriyevsky, K. Doll, G. Cakmak, M. Jansen, A. Niemer, K. Betzler, *Phys. Rev. B* **2011**, 84, 125112.
- [15] B. Andriyevsky, T. Pilz, J. Yeon, P. S. Halasyamani, K. Doll, M. Jansen, *J. Phys. Chem. Solids* **2013**, 74, 616.
- [16] X. Wang, Y. Wang, B. Zhang, F. Zhang, Z. Yang, S. Pan, *Angew. Chem. Int. Ed.* **2017**, 56, 14119–14123; *Angew. Chem.* **2017**, 129, 14307–14311.
- [17] G. Shi, Y. Wang, F. Zhang, B. Zhang, Z. Yang, X. Hou, S. Pan, K. R. Poeppelmeier, *J. Am. Chem. Soc.* **2017**, 139, 10645.
- [18] G. Shi, F. Zhang, B. Zhang, D. Hou, X. Chen, Z. Yang, S. Pan, *Inorg. Chem.* **2017**, 56, 344.
- [19] B. Zhang, G. Shi, Z. Yang, F. Zhang, S. Pan, *Angew. Chem. Int. Ed.* **2017**, 56, 3916; *Angew. Chem.* **2017**, 129, 3974.
- [20] T. Pilz, Dissertation, MPI Stuttgart, **2013**.
- [21] D. M. Chackraburty, *Acta Crystallogr.* **1957**, 10, 199.
- [22] M. J. R. Clark, H. Lynton, *Can. J. Chem.* **1969**, 47, 2943.
- [23] F. Liang, L. Kang, P. Gong, Z. Lin, Y. Wu, *Chem. Mater.* **2017**, 29, 7098–7102.
- [24] P. C. Burns, J. D. Grice, F. C. Hawthorne, *Can. Mineral.* **1995**, 33, 1131–1151.
- [25] E. Belokoneva, S. Stefanovich, O. Dimitrova, A. Ivanova, *Zh. Neorg. Khim.* **2002**, 47, 370.
- [26] M. J. Polinski, S. Wang, E. V. Alekseev, W. Depmeier, T. E. Albrecht-Schmitt, *Angew. Chem. Int. Ed.* **2011**, 50, 8891; *Angew. Chem.* **2011**, 123, 9053.
- [27] M. J. Polinski, D. J. Grant, S. Wang, E. V. Alekseev, J. N. Cross, E. M. Villa, W. Depmeier, L. Gagliardi, T. E. Albrecht-Schmitt, *J. Am. Chem. Soc.* **2012**, 134, 10682.
- [28] W. Sun, B.-C. Zhao, Y.-X. Huang, J.-X. Mi, *Acta Crystallogr. Sect. E* **2012**, 68, i17.
- [29] R. D. Shannon, *Acta Crystallogr. Sect. B* **1976**, 32, 751.
- [30] T. Balić-Žunić, E. Makovicky, *Acta Crystallogr. Sect. B* **1996**, 52, 78.
- [31] E. Makovicky, T. Balić-Žunić, *Acta Crystallogr. Sect. B* **1998**, 54, 766.
- [32] T. Bräuniger, T. Pilz, C. V. Chandran, M. Jansen, *J. Solid State Chem.* **2012**, 194, 245.
- [33] J. Czernek, J. Brus, *Chem. Phys. Lett.* **2016**, 666, 22.
- [34] L. van Wüllen, W. Müller-Warmuth, *Solid State Nucl. Magn. Reson.* **1993**, 2, 279.
- [35] G. L. Turner, K. A. Smith, R. Kirkpatrick, E. Oldfield, *J. Magn. Reson.* **1986**, 67, 544.
- [36] M. Bak, J. T. Rasmussen, N. C. Nielsen, *J. Magn. Reson.* **2000**, 147, 296.
- [37] R. Hoppe, *Angew. Chem. Int. Ed. Engl.* **1966**, 5, 95; *Angew. Chem.* **1966**, 78, 52.
- [38] R. Hoppe, *Angew. Chem. Int. Ed. Engl.* **1970**, 9, 25; *Angew. Chem.* **1970**, 82, 7.
- [39] R. Hübenthal, MAPLE, Program for the Calculation of the Madelung Part of Lattice Energy **1993**.
- [40] A. Radtke, G. Brown, *Am. Mineral.* **1974**, 59, 885.
- [41] S. L. Strong, R. Kaplow, *Acta Crystallogr. Sect. B* **1968**, 24, 1032.
- [42] H. Wu, H. Yu, Z. Yang, X. Hou, X. Su, S. Pan, K. R. Poeppelmeier, J. M. Rondinelli, *J. Am. Chem. Soc.* **2013**, 135, 4215.
- [43] P. Dorenbos, *J. Lumin.* **2003**, 104, 239.
- [44] W. C. Martin, R. Zalubas, L. Hagan, *Atomic Energy Levels—The Rare-Earth Elements*, Band 60 von *National Standard Reference Data Series*, U.S. Dept. of Commerce, U.S. National Bureau of Standards, **1978**.
- [45] J. Sommerdijk, A. Bril, *J. Lumin.* **1976**, 11, 363.
- [46] G. Qu, Z. Hu, Y. Wang, Q. Yang, L. Tong, *Adv. Funct. Mater.* **2013**, 23, 1232.
- [47] G. Sheldrick, *Acta Crystallogr. Sect. A* **2008**, 64, 112.
- [48] R. Dovesi, V. R. Saunders, C. Roetti, R. Orlando, C. M. Zicovich-Wilson, F. Pascale, B. Civalleri, K. Doll, N. M. Harrison, I. J. Bush, P. D'Arco, M. Llunell, M. Causà, Y. Noël, *CRYSTAL14 User's Manual*, University of Torino, Torino, Italy, **2014**.
- [49] R. Dovesi, R. Orlando, A. Erba, C. M. Zicovich-Wilson, B. Civalleri, S. Casassa, L. Maschio, M. Ferrabone, M. D. L. Pierre, P. D'Arco, Y. Noël, M. Causà, M. Rérat, B. Kirtman, *Int. J. Quantum Chem.* **2014**, 114, 1287.
- [50] J. P. Perdew, K. Burke, M. Ernzerhof, *Phys. Rev. Lett.* **1996**, 77, 3865.
- [51] S. H. Vosko, L. Wilk, M. Nusair, *Can. J. Phys.* **1980**, 58, 1200.
- [52] S. Grimme, *J. Comput. Chem.* **2006**, 27, 1787.
- [53] R. Orlando, R. Dovesi, C. Roetti, V. R. Saunders, *J. Phys. Condens. Matter* **1990**, 2, 7769.
- [54] J. Scaranto, S. Giorgianni, *J. Mol. Struct.: THEOCHEM* **2008**, 858, 72.
- [55] R. Nada, C. R. A. Catlow, C. Pisani, R. Orlando, *Modell. Simul. Mater. Sci. Eng.* **1993**, 1, 165.
- [56] A. Mahmoud, A. Erba, K. E. El-Kelany, M. Rérat, R. Orlando, *Phys. Rev. B* **2014**, 89, 045103.
- [57] P. Canepa, R. M. Hanson, P. Ugliengo, M. Alfredsson, *J. Appl. Crystallogr.* **2011**, 44, 225.